Atmos. Meas. Tech. Discuss., doi:10.5194/amt-2017-9, 2017
Manuscript under review for journal Atmos. Meas. Tech.
Discussion started: 23 February 2017

Atmospheric Measurement Techniques Discussions

Comparison of hourly surface downwelling solar radiation estimated from MSG/SEVIRI and forecast by RAMS model with pyranometers over Italy

Stefano Federico[1], Rosa Claudia Torcasio[2], Paolo Sanò[1], Daniele Casella[1], Monica Campanelli[1], Jan Fokke Meirink[3], PingWang[3], Stefania Vergari[4], Henri Diémoz[5], Stefano Dietrich[1]

(1) ISAC-CNR, via del Fosso del Cavaliere 100, 00133 Rome, Italy
(2) ISAC-CNR, zona Industriale comparto 15, 88046 Lamezia Terme, Italy
(3) Royal Netherlands Meteorological Institute (KNMI), Utrechtseweg 297, De Bilt, The Netherlands
(4) Technical Centre for Meteorology (CTM), ITAF, Italy
(5) ARPA Valle D'Aosta, Italy

ABSTRACT

In this paper, we evaluate the performance of two Global Horizontal solar Irradiance (GHI) estimates, one derived from Meteosat Second Generation (MSG) and another from one-day forecast of the Regional Atmospheric Modeling System (RAMS) mesoscale model. The horizontal resolution of the MSG-GHI is 3*5 km^2 over Italy, which is the focus area of this study. For this paper, RAMS has the horizontal resolution of 4km.

The performance of MSG-GHI estimate and RAMS-GHI one-day forecast are evaluated for one year (1 June 2013 – 31 May 2014) against data of twelve ground based pyranometers over Italy spanning a range of climatic conditions, i.e. from maritime Mediterranean to Alpine climate.

Statistics on hourly GHI and daily integrated GHI are presented for the four seasons and the whole year for all the measurement sites. Different sky conditions are considered in the analysis.

Results on hourly data show an evident dependence on the sky conditions, with the Root Mean Square Error (RMSE) increasing from clear to contaminated, and to overcast conditions. The RMSE increases substantially for Alpine stations in all the seasons, mainly because of the increase of the cloud coverage for these stations, which is not well represented at the satellite and model resolutions.

Considering the yearly statistics for the RAMS model, the RMSE ranges from 152 W/m^2 (31%) obtained for Cozzo Spadaro, a maritime station, to 287 W/m^2 (82%) for Aosta, an Alpine site. Considering the yearly statistics for MSG-GHI, the minimum RMSE is for Cozzo Spadaro (71 W/m^2, 14%), while the maximum is for Aosta (181 W/m^2, 51%). The Mean Bias Error (MBE) shows the tendency of RAMS to over forecast the GHI, while no specific tendency if found for MSG-GHI.

Atmos. Meas. Tech. Discuss., doi:10.5194/amt-2017-9, 2017
Manuscript under review for journal Atmos. Meas. Tech.
Discussion started: 23 February 2017

Results for daily integrated GHI show a reduction of the RMSE of at least 10%, compared to hourly GHI evaluation, for both RAMS-GHI one-day forecast and MSG-GHI estimate. A partial compensation of underestimation and overestimation of the GHI contributes to the RMSE reduction. Furthermore, a post-processing technique, namely Model Output Statistics (MOS), is applied to hourly and daily integrated GHI. The application of MOS shows an improvement for RAMS-GHI up to 24%, depending on the site considered, while the impact of MOS on MSG-GHI RMSE is small (2-3%).

1. Introduction

The Global Horizontal Irradiance (GHI) is the power of the solar spectrum reaching the surface and it is a key parameter for several disciplines (Ceamanos et al, 2014; Sánchez et al, 2014). In particular, the exploitation of solar energy, which is the most abundant renewable energy, is of great interest because the larger penetration of renewable energies into the energy market would reduce the emissions of greenhouse gases (Szuromi et al 2007; IEA, 2010; EWEA, 2011) caused by human activities.

Photovoltaic (PV) systems enable the conversion of the GHI into electricity through semi-conductor devices and, in order to control the increase of global temperature, PV systems are expected to have a potential by more than 200 GW by 2020 (EWEA, 2011).

For the operation and implementation of PV systems, observations and forecast of GHI play a major role. Surface weather stations equipped with a pyranometer give reliable observations of GHI, but they are often unavailable in the places where new installations are planned. For this purpose, the GHI may be derived from other sources, as the Meteosat Second Generation (MSG) Spinning Enhanced Visible and Infrared Imager (SEVIRI) or a Numerical Weather Prediction Model (NWP).

In this paper, we show the performance of both the MSG-GHI estimate, following the methodology of Greuell et al. (2013), and RAMS-GHI one-day forecast over the whole Italian territory. To verify GHI, we use twelve pyranometers, which are representative of sites with very different climates, from Mediterranean maritime to Alpine. Moreover, the study spans a whole year to properly account for the natural variability of the Mediterranean climate.

Many studies are available on the performance of different approaches to estimate and forecast solar radiation in several countries in Europe (Roebeling et al, 2008; Greuell et al, 2013; Lara-Fanego et al., 2012; Kosmopulos et al., 2015; Gómez et al., 2016; Lorenz et al, 2009; Perez et al, 2006; Rincon et al, 2011), because the planning of new PV systems and the managing of the electricity grid with large amounts of production from solar energy requires the knowledge and forecast of

GHI with high accuracy. This study goes in this direction by considering a nation-wide evaluation for a whole year. Moreover, Italy has a great potential for the exploitation of solar energy (Petrarca et al., 2000).

We consider both the hourly and daily integrated GHI, the latter being the GHI integrated for each day for the different datasets, to evaluate the performance of both RAMS-GHI and MSG-GHI for two different timescales of interest. Also, we show the impact of a simple post processing technique, which aims to reduce the Mean Bias Error (MBE) for each site, on the GHI estimate and forecast.

The paper is organized as follows: Section 2 shows the dataset used and the methodology adopted to evaluate the errors of the MSG-GHI estimate and RAMS-GHI one-day forecast; Section 3 shows the results considering both the hourly and daily integrated GHI; Conclusions are given in Section 4.

2. Data and methods

2.1 Cloud properties and GHI from MSG-SEVIRI

The SEVIRI instrument onboard MSG carries 11 channels in the visible to infrared spectral range with a spatial resolution of 3x3 km^2 at the sub-satellite point and a temporal repeat frequency of 15 minutes. Over Italy the spatial resolution is about 3x5 km^2. From the SEVIRI measurements, a range of cloud physical properties can be derived with the Cloud Physical Properties (CPP) algorithm. The algorithm first identifies cloudy and cloud contaminated pixels using a series of thresholds and spatial coherence tests on the measured visible and infrared radiances (Roebeling et al., 2008). So, depending on the tests, the sky can be classified as clear, contaminated or overcast. Subsequently, cloud optical properties (optical thickness and particle size) are retrieved by matching observed reflectances at visible (0.6 μm) and near-infrared (1.6 μm) wavelengths to simulated reflectances of homogeneous clouds composed of either liquid or ice particles. The thermodynamic phase (liquid or ice) is determined as part of this procedure, using a cloud-top temperature estimate as additional input (Roebeling et al., 2008; Stengel et al., 2014).

Building on the retrieval of cloud physical properties, the Surface Insolation under Clear and Cloudy Skies (SICCS) was developed to estimate surface downwelling solar radiation using broad-band radiative transfer simulations (Deneke et al., 2008; Greuell et al., 2013). Both global irradiance as well as the direct and diffuse components are retrieved. While the cloud properties are

Atmospheric Measurement Techniques Discussions

the main input for cloudy and cloud-contaminated pixels, information about atmospheric aerosol from the Monitoring Atmospheric Composition and Climate (MACC) project is used for cloud-free scenes. Greuell et al. (2013) performed an extensive validation of the MSG-SICCS retrievals with Baseline Surface Radiation Network (BSRN) ground-based observations in Europe for the year 2006. They found median values of the station GHI biases of +7 W/m2 (+2%) and hourly GHI RMSEs of 65 W/m^2 (18%).

The CPP and SICCS products are publicly available at msgcpp.knmi.nl.

2.2 The RAMS set-up

In this paper, we evaluate the performance of the RAMS-GHI one-day forecast. The model is run with two one-way nested grids (Table 1, Figure 1). The coarser domain has 12 km horizontal resolution and covers most of Europe, while the second domain has 4 km horizontal resolution and covers the Italian peninsula. Thirty-six vertical levels, extending up to the lower stratosphere, are used in the terrain-following coordinate system of RAMS (Cotton et al., 2003).

The exchange between the atmosphere, the surface and the soil is computed by the LEAF (Land Ecosystem-Atmosphere Feedback) submodel. The LEAF submodel considers the interaction among several features, as well as their influence on the atmosphere: vegetation, soil, lakes and oceans, and snow cover.

RAMS parameterises the unresolved transport using *K*-theory, in which the covariance is evaluated as the product of an eddy mixing coefficient and the gradient of the transported quantity. The turbulent mixing in the horizontal directions relates the mixing coefficients to the fluid strain rate (Smagorinsky, 1963) and includes corrections for the influence of the Brunt-Vaisala frequency and the Richardson number (Pielke, 2002).

Convective precipitation is parameterised following Molinari and Corsetti (1985), who modified the Kuo scheme (Kuo, 1974) to account for downdrafts. The convective scheme is applied to the coarser RAMS domain, while convection is assumed explicitly resolved for the inner domain.

Explicitly resolved precipitation is computed by the WRF (Weather Research and Forecasting System) – single-moment-microphysics class 6 (WSM6) scheme (Hong et al., 2006), which was recently adapted to RAMS (Federico, 2016).

Short wave and long wave radiation is computed by the Chen and Cotton scheme (Chen and Cotton, 1983); the radiative scheme accounts for the total condensate in the atmosphere but not for the specific hydrometeor type.

Initial and boundary conditions are interpolated from the operational analysis/forecast cycle issued at 12:00 UTC by the ECMWF (European Centre for Medium range Weather Forecast). Initial and boundary conditions are available at 0.5° horizontal resolution and on nine pressure levels, from 1000 to 30 hPa.

The model was run for a whole year (1 June 2013 - 31 May 2014) with the above configuration. Each simulation lasts 36 h and starts at 12 UTC of the day before the day of interest. The first 12 h are used as spin-up time and are discarded. The model output is available hourly.

2.3 Surface observations and evaluation methodology

In this work, we consider 12 pyranometers over Italy (Figure 2). Their coordinates, height above the sea level and abbreviations used in this paper are shown in Table 2. The pyranometers span a wide range of climatic conditions: Trapani, Cozzo Spadaro, Santa Maria di Leuca, Capo Palinuro, Pratica di Mare, Cervia, Pisa and Trieste are located by the sea, and show a typical Mediterranean climate; Vigna di Valle is still characterized by a mild Mediterranean climate but it is located in more complex hilly terrain; Paganella, Monte Cimone and Aosta are mountainous stations, and this has an important impact on the RAMS and MSG performance at the sites. More specifically, Paganella is on the Alps, Monte Cimone is on the Apennines, while Aosta, with a lower altitude, is embedded in the rough Alpine terrain.

Pyranometers data are quality controlled following Zahumensky (2004). In particular, apart from the manual maintenance related to the periodical cleaning of the dome, quality controls performed over the data are:

1. Plausible value check, that is to verify if the values are within the acceptable range limits;
2. Internal consistency check, that is to verify the internal consistency of data based on the relation between two parameters, in this case solar radiation and sunshine duration (if available).

Irradiance measurements in Aosta are daily checked through comparison with clear-sky simulations by a radiative transfer model (libRadtran, Emde et al., 2016). The CMP21 radiometer is calibrated every two years at the Physikalisch-Meteorologisches Observatorium Davos/World Radiation Center (PMOD/WRC) against a member of the World Standard Group (WSG) for the direct component and a shaded standard pyranometer of the World Radiation Center (WRC) for the diffuse component. The radiometric stability was better than 0.2% over the period of the six years of measurements.

Atmos. Meas. Tech. Discuss., doi:10.5194/amt-2017-9, 2017
Manuscript under review for journal Atmos. Meas. Tech.
Discussion started: 23 February 2017

The different environmental characteristics of the stations in terms of sky conditions are presented in Table 3, which shows for each station and season, as well as for the whole year, the percentage of data in clear, contaminated and overcast conditions, classified by the methodology of Section 2.1.

There is a considerable variability of the sky conditions with the season for each station. For Trapani, for example, the percentage of clear sky in summer is 82%, while it reduces to 38% in fall and 48% in winter. Also, for each season, the variability of the sky conditions with the stations is high. For maritime stations, for example, the percentage of clear skies in summer is above 70% with few exceptions, while it reduces to 45, 34, 32% for Paganella, Monte Cimone and Aosta, respectively.

The RAMS GHI forecast is available hourly and the common frequency of pyranometer observations and MSG-GHI estimate (every half an hour) was reduced to the hourly basis. Starting from these data, the MBE (Mean Bias Error) and the RMSE (Root Mean Square Error) were computed:

$$MBE = \frac{1}{N}\sum_{i=1}^{N}(x_{fi} - x_{oi})$$

$$RMSE = \sqrt{\frac{1}{N}\sum_{i=1}^{N}(x_{fi} - x_{oi})^2}$$

Where x_f is the RAMS forecast or the MSG GHI estimate, x_o is the pyranometer observation, and N is the total number of data available for the statistic.

In addition to the MBE and RMSE computed from hourly data, the statistics are computed starting from daily data. In this case, the integral of the GHI for the whole day is first computed for each dataset, then the MBE and RMSE are computed from the daily data.

Relative MBE and relative RMSE error measures (rMBE, rRMSE) are also used. The normalization is done with the pyranometer observation for the station and period considered, i.e. :

$$rMBE = 100\frac{\sum_{i=1}^{N}(x_{fi} - x_{oi})}{\sum_{i=1}^{N} x_{oi}}$$

$$rRMSE = 100\,\frac{\sqrt{\frac{1}{N}\sum_{i=1}^{N}(x_{fi} - x_{oi})^2}}{\frac{1}{N}\sum_{i=1}^{N} x_{oi}}$$

3. Results

3.1 General considerations on MSG estimate and RAMS forecast

Figure 3a shows the scatter-plot for the GHI estimate of MSG and the pyranometer for Vigna di Valle, using hourly GHI. The black dots refer to clear sky, while the red dots are for contaminated and overcast conditions (after also referred to as cloudy conditions) for the entire yearly dataset. Three regression curves are shown: the black one is for clear conditions, the red one is for cloudy conditions (both contaminated and overcast) and the blue one is for the whole dataset. The parameters of the linear regressions are shown in the respective colours: *a* is the slope, *b* is the intercept, *r* is the correlation coefficient, *N* is the number of data. The probability to have a correlation coefficient larger than that found by chance is also shown ($p>r$). A small value of this probability shows a high significance of the regression. From Figure 3a it is apparent the larger scatter of the data for cloudy conditions compared to clear sky. This is confirmed by the correlation coefficient, which is 0.96 for clear sky and 0.89 for contaminated and overcast conditions. Also, the slope (intercept) of the linear regression is closer to 1.0 (closer to 0.0) for clear sky, in better agreement with the perfect regression.

Considering Figure 3a, two kinds of error are evident: a) there are cases when the cloud classification by MSH-GHI is wrong as, for example, for the black dots in the lower-right part of Figure 3a. For these points, the MSH-GHI is high (larger than 600 W/m^2) while the pyranometer observation is below 300 W/m^2. This error becomes particularly important for mountainous stations because, when the soil is covered by snow, it is more difficult for the MSG-GHI algorithm to correctly identify the clouds; b) the larger scatter for cloudy conditions compared to clear sky data is a consequence of the difficulty to correctly estimate the cloud optical depth, which can result in both overestimation of the MSG-GHI, i.e. the cloud optical depth is underestimated, or underestimation of the MSG-GHI, i.e. the cloud optical depth is overestimated. It is important to note that also red points may contain cases of wrong cloud classification. Nevertheless, the larger spread of the red points compared to the black ones shows, indirectly, the overall good classification of the sky conditions by MSG because the estimation of the GHI is more difficult for cloudy skies.

Figure 3b shows the scatter plot for the same station for the RAMS-GHI one-day forecast. It is apparent the larger scatter compared to MSG for both clear and cloudy conditions. The correlation coefficient of the linear fit is 0.91 for clear conditions, while it is 0.60 for contaminated and overcast sky, showing a rather poor performance of the RAMS-GHI one-day forecast in cloudy conditions. Both values are lower than the corresponding values of the MSG-GHI estimate.

Figure 3b for clear sky shows cases when RAMS predicts clouds that are not observed, i.e. the black dots in the upper left part of the figure, and cases when RAMS does not predict clouds that are observed, i.e. the black dots in the lower-right part of the figure. Also, the large scatter of red dots shows either cases of incorrectly predicted sky conditions or errors in the representation of the cloud optical depth.

From Figure 3 it follows that: a) the performance in clear conditions is better compared to cloudy sky; b) the estimate of the GHI by MSG outperforms the RAMS forecast. These results, even if shown for Vigna di Valle are found for all stations considered in this paper, and are similar to the findings of several studies (Kosmopulos et al., 2015; Lara-Fanego et al., 2012; Gomez et al., 2016). Moreover, because of the dependence of the performance on the sky condition, a large variability of the performance is expected with the seasons and with the stations, because the cloud coverage at each site varies with the season and, for each season, from site to site. This point is investigated in the following sections.

3.2 Performance dependence on the season and cloud cover

Figure 4a shows the MBE of the MSG-GHI hourly estimate in all sky conditions for the different seasons, for the whole year and for all stations. Focusing on the whole year, there are five stations where the GHI is overestimated (maximum value at Monte Cimone; 18 W/m^2) and seven stations where the GHI is underestimated (minimum value at Pratica Di Mare; -12 W/m^2). The MBE is, however, rather small in absolute value and it is lower than 10 W/m^2 for seven pyranometers. Considering the variability of the results with the station in all seasons, we note the larger absolute values for mountainous stations. This is expected because there are a larger number of cloudy data for those stations (Table 3), and the performance of the GHI estimate by MSG is worse for cloudy conditions (Figure 3a). This result is general and applies also to the RAMS forecast.

Figure 4b shows the MBE for the RAMS one-day forecast. Considering the statistics for the whole year it is noted that the values are in general positive and below 30 W/m^2, with the exceptions of Paganella and Aosta where the MBE is negative, i.e. the RAMS forecast underestimates the GHI, and reaches the huge value of -120 W/m^2. The same behavior is found for all seasons, with few exceptions. Excluding the mountainous stations of Aosta and Paganella, the largest MBE is found in summer, showing the tendency of the RAMS forecast to overestimate the GHI in this season, while the smallest values occur in spring. Considering the dependence of the MBE with the station, it is evident the worse performance for mountainous stations, namely Paganella and Aosta, compared to maritime stations. The inspection of the model output for those stations reveals that the

Atmos. Meas. Tech. Discuss., doi:10.5194/amt-2017-9, 2017
Manuscript under review for journal Atmos. Meas. Tech.
Discussion started: 23 February 2017

Atmospheric Measurement Techniques Discussions

main source of errors was the over forecast of cloudy conditions. It is not easy to find the reason for this behavior, because it is caused by several factors as errors in the physical, especially microphysical and radiative, and numerical parameterizations of the model, and errors in the initial and boundary conditions. Also, the 4 km horizontal resolution is not enough to resolve the fine orographic structures over the Alps (Aosta and Paganella) and over the Apennines (Monte Cimone), and their interaction with large scale atmospheric systems. This causes a misrepresentation of the local circulations and atmospheric conditions, both forced locally or generated by the interaction of large scale flow with the orography, which gives large errors for mountainous stations.

Figure 5a shows the RMSE for the MSG-GHI hourly estimate in all sky conditions for different seasons, for the whole year and for the twelve stations. Considering the whole year, we note two groups of stations: the first with values around 100 W/m^2 containing the maritime and hilly stations, the second with values larger than 150 W/m^2 containing the mountainous stations. It is important to note that the 3*5km^2 horizontal resolution of the MSG-GHI can be not enough to represent the local sky conditions at the pyranometer, especially for mountainous stations where the complex orography determines rapid changes of the cloud coverage in short distances. As a consequence, the sky conditions cannot be well represented causing larger errors for mountainous stations. The different performance of the two groups of stations is confirmed for all the seasons and highlights the difficulty to clearly distinguish and classify clouds for the specific sites.

Considering the behavior of the RMSE with the season, the lowest values are often found in winter even if the performance does not vary sizably with the season. Winter has also the lowest RMSE averaged over all stations (84 W/m^2), followed by fall (98 W/m^2), summer (118 W/m^2), and spring (125 W/m^2). The performance in winter is better compared to other seasons because the RMSE statistic is sensitive to the larger errors (Wilks, 2006), and the departures of the GHI estimate from the observation is lower in winter because the GHI is smaller. It is also noted the larger variability of the performance in summer compared to other seasons, which will be discussed later on in this section.

Another interesting statistic to quantify the performance of the MSG-GHI estimate is the rRMSE, which is shown in Table 4. Considering the whole year, this value ranges from 14% of Cozzo Spadaro to 53% of Monte Cimone; for maritime and hilly stations the rRMSE is below 30%, while it is above 40% for mountainous stations, showing again the difference between the two groups. The RMSE has the smallest value in summer and the highest value in winter. While this result is in part determined by the larger observed values of the GHI in summer, the statistic shows more clearly the impact of the cloud coverage on the MSG-GHI performance. The percentage of cloudy conditions is larger in winter compared to summer for all stations (Table 3) and the error of the MSG-GHI increases in cloudy conditions, as shown by the rRMSE. However, the larger differences between the MSG-GHI estimate and the pyranometer observation in summer, even if in fewer occasions, determine larger value of the RMSE compared to winter, as shown in Figure 5a.

Figure 5b shows the RMSE for the RAMS-GHI one-day forecast. Considering the whole year, the RMSE is below 200 W/m^2 for all stations with the exception of the mountainous stations. This is caused by the difficulty of the RAMS forecast to correctly predict the cloud coverage for those stations. Considering the RMSE behavior for different seasons, averaged for all stations, the lowest error is found in winter (142 W/m^2) followed by fall (171 W/m^2), summer (186 W/m^2) and spring (245 W/m^2). Summer has the largest RMSE spread among the stations. In particular, it shows the lowest error among all stations and seasons (Cozzo Spadaro, 110 W/m^2) but also values larger than 300 W/m^2 for Paganella and Aosta. This result is caused by the RMSE statistics, which is sensitive to large differences between the RAMS-GHI one-day forecast and observations. These differences are the largest in summer (the lowest in winter) when the forecast of the cloud coverage is incorrect, causing the largest spread of the performance among stations. This applies also to the MSG-GHI estimate.

The RMSE of the RAMS-GHI one-day forecast is more than twice that of the MSG-GHI considering both the whole year and the seasons. The mountainous stations are an exception also in this case because the performance of MSG and RAMS are closer. A better performance of the MSG-GHI estimate is expected, because it is derived from the observations, while the RAMS is a forecast, however the results of this section quantify the difference between the two GHI sources in different conditions.

The rRMSE for the RAMS-GHI is shown in Table 5. Considering the yearly statistic, the values range from 31% for Cozzo Spadaro to 81% for Aosta. The rRMSE varies considerably between the mountainous stations compared to maritime and hilly stations, jumping from 53% obtained for Trieste (the worst performance for maritime and hilly stations) to 72% of Paganella (the best performance for mountainous stations). The variability of the rRMSE with the seasons shows again the important impact of the cloud coverage on the RAMS-GHI one-day forecast performance. The smallest rRMSE are in summer, and the largest in winter for all stations. Moreover, for Trieste, Cimone and Aosta the rRMSE is about 100 % or larger in winter.

Up to this point we discussed the MBE and RMSE performance as a function of the seasons and stations for all sky conditions, which showed the dependence of the performance, both of MSG-

GHI estimate and RAMS-GHI forecast, on the cloud coverage. To better focus on this point, Figure 6 shows the RMSE as a function of the cloud coverage for MSG-GHI (Figure 6a) and for RAMS-GHI forecast (Figure 6b).

In Figure 6a, the colored bars for each sky condition (1=clear, 2=contaminated and 3=overcast) show the GHI average for the pyranometers, while the gray bars in the background show the RMSE of the MSG-GHI estimate for the different sky conditions. The GHI average depends on the data availability in different seasons. For example, considering clear sky, the GHI in Palinuro and Cozzo Spadaro is larger than those of other maritime stations in Southern Italy. This is determined by the larger fraction of available data in summer for Palinuro and Cozzo Spadaro compared to other pyranometers.

Figure 6a shows that the GHI decreases for the sky changing from clear to contaminated and to overcast conditions, while the RMSE increases as the sky conditions become cloudier. More specifically, the RMSE is between 50 and 150 W/m^2, depending on the station, for clear sky, between 50 and 200 W/m^2 for contaminated conditions, and between 80 and 200 W/m^2 for overcast conditions.

Figure 6b shows the performance of the RAMS-GHI forecast as a function of the sky conditions. The values of the pyranometers are the same as in Figure 6a and are shown to help comparison. The RAMS-GHI one-day forecast RMSE increases from clear to overcast conditions and the error increases compared to MSG-GHI. More specifically, excluding mountainous stations, the RMSE is 100 W/m^2 for clear sky, 150-250 W/m^2, depending on the station, for contaminated sky, and around 250 W/m^2 for overcast conditions. In the latter case the RMSE is larger than the GHI for most stations, i.e. the relative error is larger than 100%.

Before concluding this section, it is interesting to compare the RAMS-GHI one-day forecast with the one-day (1D) persistence forecast (Table 6), which is given by assuming that the GHI forecast for tomorrow is the GHI recorded today. Considering the yearly statistics, the RAMS-GHI gives better performance of the 1D-persistence forecast for all pyranometer but Paganella. The improvement given by the RAMS forecast is larger than 10% of the RMSE, showing a sizable impact. However, for Aosta, the difference between the two forecasts is negligible.

Considering the performance of the RAMS-GHI and 1D persistence forecasts with the seasons, we note that: a) in winter the performance of the 1D persistence forecast is better than the RAMS-GHI one-day forecast for seven pyranometers. This results is obtained for six stations in fall, four stations in spring and one station in summer; b) for mountainous stations the 1D persistence

Atmos. Meas. Tech. Discuss., doi:10.5194/amt-2017-9, 2017
Manuscript under review for journal Atmos. Meas. Tech.
Discussion started: 23 February 2017

forecast is better than the RAMS-GHI one-day forecast for most-cases. These results show again the important impact of the cloud-coverage on the performance of the RAMS-GHI one-day forecast, nevertheless the RAMS forecast can give added valued to the GHI one-day forecast in most cases.

3.3 Daily evaluation and MOS application

In this section, we first discuss the impact of the time interval on the RAMS-GHI and MSG-GHI performance, then we consider the impact of a simple post-processing technique, the Model Output Statistics (MOS), to improve the RAMS-GHI and MSG-GHI performance for daily integrated GHI.

Figure 7a shows the rRMSE for different stations and seasons for the RAMS-GHI one-day forecast. This figure is still computed from hourly data, as in the previous section (Figure 6b), but the RMSE is expressed in percentage to help comparison among statistics presented in this section.

Figure 7b shows the rRMSE for daily integrated GHI. Comparing the result of Figures 7a and 7b, it is apparent the impact of the time interval on the rRMSE. Considering the yearly result, for example, the rRMSE is reduced by more than 9% for all stations when the statistics are computed for daily integrated GHI, and for several stations the improvement is larger than 15%. This improvement is found for all seasons and stations. In addition to the way used to compute the statistic, which produces smaller values compared to the same statistic from hourly data, the improvement is also caused by a partial compensation of the forecast underestimation and overestimation of the GHI during the day.

Considering the rRMSE for the MSG-GHI, a similar improvement is found, when computed for daily integrated GHI (Table 4). For the yearly statistics, the rRMSE decreases by 10% or more for all stations and an improvement larger than 5% is found in all seasons with a considerable variation among the stations.

The last problem considered in this paper is the impact of the Model Output Statistics (MOS) on the one-day RAMS-GHI forecast.

The MOS technique is used to reduce the MBE of the RAMS-GHI forecast and MSG-GHI estimate. The MBE is caused by both the approximations in the meteorological model and in the methodology used to estimate GHI from MSG data, and by the horizontal grid used to represent the real world, which smoothens the surface features causing systematic errors.

The MOS consists of a linear regression computed between the GHI forecast (or estimate) and observation for a training period:

$$y=a+bx \quad (1)$$

where x is the RAMS-GHI one-day forecast (or MSG estimate) and y is the pyranometer observation.

The MOS was computed for each season and the "leave one" methodology was used to verify the forecast using MOS. In this method, the Eqn. (1) is computed considering all data but one (actual data), and it is applied to the actual data to give the corrected forecast. Because the MOS is computed starting from hourly data, the training period is all the season but one hour. This procedure was repeated for all the hourly data, then the RMSE and rRMSE were computed.

The statistic computed from hourly data are shown in Table 6 for the RAMS forecast. It is apparent that the MOS improves the RAMS performance especially for Aosta and Paganella, where the Bias was high (Figure 4b). In particular, after the MOS application, the absolute value of the Bias is less than 30 W/m^2 for Paganella and Aosta for all seasons as well as for the whole year (not shown). With the MOS application, the RAMS-GHI one-day forecast performs better than the 1D persistence forecast for all stations considering the whole year, even if there are still occasions when the 1D persistence forecast has a better performance than the RAMS-GHI one-day forecast (Paganella in winter and fall, Aosta in winter, spring and fall, Trapani in winter). This result confirms that the forecast of the GHI in cloudy conditions is a big issue for the RAMS model.

Starting form hourly data after the MOS correction, daily integrated GHI statistics were also computed. The rRMSE of RAMS-GHI one-day forecast after the MOS application for the daily integrated GHI is shown in Figure 7c and Table 5. The rRMSE decreases by 2-8% for most stations compared to the daily integrated GHI without MOS, with exception of Paganella and Aosta, where the improvement is larger. This is expected because the Bias is larger for these stations (Figure 4b) and the MOS is a technique that improves the forecast by reducing the Bias. This is confirmed by the inspection of the rMBE (not shown), which is reduced by the application of the MOS.

The application of the MOS to the MSG-GHI gives no improvement on both rRMSE (Table 4) and rMBE (not shown). This is caused by the small values of the Bias of the MSG-GHI (Figure 4a).

4. Conclusions

Atmos. Meas. Tech. Discuss., doi:10.5194/amt-2017-9, 2017
Manuscript under review for journal Atmos. Meas. Tech.
Discussion started: 23 February 2017

Atmospheric Measurement Techniques Discussions

In this paper, we analyzed the performance of the MSG-GHI estimation and RAMS-GHI one-day forecast for one year (1 June 2013 - 31 May 2014) over the Italian territory. Twelve pyranometers, scattered over the country and representing a variety of climate characteristics, were used to evaluate the performance. The analysis was performed for both hourly and daily integrated GHI, and the dependence with the season and sky conditions was studied.

The results for the hourly analysis show a marked dependence of the MSG-GHI estimation and RAMS-GHI one-day forecast on the sky conditions, which mirrors in a notable dependency with the season and station. In particular, mountainous stations have worse performance compared to hilly and maritime stations.

The analysis of the MBE for the RAMS-GHI shows that the one-day forecast overestimates the GHI, with the exception of the mountainous stations of Paganella and Aosta, where a considerable underestimation is found. The MSG-GHI doesn’t show a specific behavior of the MBE with both overestimation and underestimation, depending on the season and station.

The RMSE for the RAMS-GHI one-day forecast is the lowest in winter, followed by fall and spring. In summer, the RMSE shows the largest difference among the stations, the maritime stations showing the best performance, because the RMSE is sensitive to the departures between forecast and observation, which are larger in summer when the cloud coverage is not well predicted or estimated at the site.

The RMSE of the MSG-GHI estimate is more than halved compared to RAMS-GHI, with the exception of the mountainous stations where the RMSE of the two datasets are closer. The seasonal behavior of the MSG-GHI RMSE shows a minimum in winter, but the differences among the seasons are lower compared to the RAMS forecast.

The analysis of the rRMSE reveals more clearly the impact of the cloud coverage on the performance. Both RAMS-GHI one-day forecast and MSG-GHI estimate show the largest rRMSE in winter and the lowest in summer, following the behavior of the cloud coverage. It is also noted that the rRMSE of the RAMS-GHI one-day forecast for Trieste, Cimone and Aosta is about 100 % in winter.

The cloud coverage has, however, an important impact also on the RMSE of both MSG-GHI estimate and RAMS-GHI one-day forecast. The error increases as the cloud coverage increases. This is especially evident for RAMS because the RMSE averaged over all the stations varies from 91 W/m^2, to 191 W/m^2, and to 245 W/m^2 for clear, contaminated and overcast conditions, respectively; for MSG-GHI, the RMSE averaged over all stations varies from 68 W/m^2, to 123 W/m^2, and to 98 W/m^2 for clear, contaminated and overcast conditions, respectively.

The increase of the RMSE with the cloud coverage is determined not only by the inability of the radiative scheme to compute the GHI in cloudy conditions, but also by the inability of the two methods to correctly represent the cloud coverage. In general, the large errors of the RAMS-GHI one-day forecast and those of the MSG-GHI estimation show that the horizontal resolutions of both data sources it is not enough to represent the complex orographic features of the mountainous pyranometers.

The results for daily integrated GHI show a notable improvement of the RAMS-GHI and MSG-GHI performance, because the RMSE computed for daily integrated GHI is reduced by more than 10% compared to the same statistic computed from hourly data. In addition to the methodology used to compute the statistic, the partial compensation of overestimation and underestimation during the day improves the performance for the daily integrated GHI. This result is similarly shown in other studies in different countries (Lara-Fanego et al., 2012; Kosmopulos et al., 2015; Gómez et al., 2016).

Applying a simple post-processing technique, i.e. the MOS, to the RAMS-GHI one-day forecast reduces the RMSE (2-8% of its value, depending on the station, for daily integrated GHI), while the MOS has a negligible impact on the MSG-GHI RMSE. This result is expected considering that the RAMS-GHI has a larger bias compared to MSG-GHI and the MOS improves the RMSE by reducing the bias.

The performance of the RAMS-GHI one-day forecast, with and without the MOS application, has been compared with the 1D persistence forecast to quantify the added value of the RAMS forecast. The results show, in general, that the RAMS forecast outperforms the 1D persistence forecast and that the improvement is often larger than 10% of the RMSE. Nevertheless, the 1D persistence forecast has a better performance than RAMS-GHI one-day forecast for mountainous stations and, for specific seasons, for other pyranometers. The application of the MOS improves the RAMS-GHI one-day forecast performance, nevertheless there are still few occasions (Paganella in winter and fall, Aosta in winter, spring and fall, and Trapani in winter) when the 1D persistence forecast outperforms the RAMS forecast.

Overall, the results of this paper show that the MSG-GHI estimate and the RAMS forecast have still big issues in cloudy conditions. In particular, considering the potential of the RAMS forecast to participate to the energy market, it is difficult to assess its usefulness from the results of this paper.

While the RAMS forecast outperforms the 1D persistence forecast in clear sky, it has large errors in cloudy conditions and it is not easy to give a final balance between the advantages in clear conditions and disadvantages in cloudy conditions. Considering also the variability of the RAMS performance from site to site, the usefulness of the RAMS forecast from an economic perspective must be evaluated from case to case (Wittman et al. 2008).

Acknowledgments

The ECMWF and CNMCA (Centro Nazionale di Meteorologia e Climatologia Aeronautica) are acknowledged for the use of the MARS (Meteorological Archive and Retrieval System).

References

Ceamanos, X., Carrer, D., Roujean, J.-L., "Improved retrieval of direct and diffuse downwelling surface shortwave flux in cloudless atmosphere using dynamic estimates of aerosol content and type: Application to the LSA-SAF project", *Atmospheric Chemistry and Physics*, 14, 8209–8232, 2014.

Chen C., Cotton W.R., "A One-Dimensional Simulation of the Stratocumulus-Capped Mixed Layer", *The Boundary Layer Meteorology*, 25, 289–321, 1983.

Cotton W. R., Pielke R. A. Sr., Walko R. L., Lista D. E., Tremback C. J., Jiang H., McAnelly R. L., Harrington J. Y., Nicholls M. E., Carrio G. G., McFadden J. P., "RAMS 2001: Current status and future directions", *Meteorology and Atmospheric Physics*, 82, 5-29, 2003.

Deneke H. M., A.J. Feijt, and R.A. Roebeling, "Estimating Surface Solar Irradiance from METEOSAT SEVIRI-derived Cloud Properties", *Remote Sensing of Environment*,112 (6), 3131-3141, 2008.

Emde, C., Buras-Schnell, R., Kylling, A., Mayer, B., Gasteiger, J., Hamann, U., Kylling, J., Richter, B., Pause, C., Dowling, T., and Bugliaro, L.: The libRadtran software package for radiative transfer calculations (version 2.0.1), Geosci. Model Dev., 9, 1647-1672, doi:10.5194/gmd-9-1647-2016, 2016

EWEA, The European Wind Energy Association, "EU Energy Policy to 2050: achieving 80-95% emissions reductions", March 2011.

Federico S., “Implementation of the WSM5 and WSM6 Single Moment Microphysics Scheme into the RAMS Model: Verification for the HyMeX-SOP1”, *Advances in Meteorology*, Volume 2016, Article ID 5094126,17 pages, 2006. http://dx.doi.org/10.1155/2016/5094126.

Gómez I., Caselles V., and Estrela M. J., “Seasonal Characterization of Solar Radiation Estimates Obtained from a MSG-SEVIRI-Derived Dataset and a RAMS-Based Operational Forecasting System over the Western Mediterranean Coast”, *Remote Sensing*, 8(1),46, 2016. doi:10.3390/rs8010046

Greuell, W., Meirink J.F. and Wang P., “Retrieval and validation of global, direct, and diffuse irradiance derived from SEVIRI satellite observations”, Journal of Geophysical Research, 118, 2340-2361, 2013.

doi:10.1002/jgrd.50194 <http://dx.doi.org/10.1002/jgrd.50194>.

Hong S.Y. and Lim J.J.O., “The WRF single-moment 6-class microphysics scheme (WSM6)”, *Journal of the Korean Meteorological Society*, vol. 42, pp. 129–151, 2006.

IEA, Electricity information, Published by the International Energy Agency, p. 762, 2010.

Kosmopoulos P.G., Kazadzis S., Lagouvardos K., Kotroni V., Bais A, “Solar energy prediction and verification using operational model forecasts and ground-based solar measurements”, *Energy*,93,1918-1930, 2015.

Kuo H. L., “Further Studies of the Parameterization of the Influence of Cumulus Convection on Large-Scale Flow”, *Journal of Atmospheric Sciences*, 31, 1232–1240, 1974.

Lara-Fanego V., Ruiz-Arias J.A., Pozo-Vazquez D. , Santos-Alamillos F.J., Tovar-Pescador J., “Evaluation of the WRF model solar irradiance forecasts in Andalusia (southern Spain) ”, *Solar Energy*,86, 2200–2217, 2012.

Lorenz E, Remund J, Muller C, Traunmuller W, Steinmaurer G, Pozo D, Ruiz-Arias J.A., Fanego V.L., Ramirez L., Romeo M.G., Kurz C., Pomares L.M., Guerrero C., “Benchmarking of different approaches to forecast solar irradiance”, *EUPVSEC proceedings*, p. 4199e208, 2009. http://dx.doi.org/10.4229/24thEUPVSEC2009-5BV.2.50.

Molinari J., and Corsetti T., “Incorporation of cloud-scale and mesoscale down-drafts into a cumulus parametrization: results of one and three-dimensional integrations”, *Monthly Weather Review*, 113, 485-501, 1985.

Perez R., Moore K., Wilcox S., Renne D., Zelenka A., “Forecasting solar radiation e preliminary evaluation of an approach based upon the national forecast database”, *Solar Energy* 81,809-12, 2006.

Petrarca S., Cogliani E., Spinelli, F., "La radiazione solare globale al suolo in Italia" *Enea, Rome*, 193 pp, 2000.

Pielke R. A., "Mesoscale Meteorological Modeling", *Academic Press, San Diego*, 676 pp, 2002.

Rincon A., Jorba O., Baldasano J.M., Della Monache L., "Assessment of short-term irradiance forecasting based on post-processing tools applied on WRF meteorological simulations", *ES1002: Workshop*, March 22-23, 2011.

Roebeling R. A., Deneke H. M., and Feijt A. J., "Validation of cloud liquid water path retrievals from SEVIRI using one year of CloudNET observations", *Journal of Applied Meteorology and Climatology*, 47, 206–222, 2008.

Sánchez, J.M., López-Urrea, R., Rubio, E., González-Piqueras, J., Caselles, V., "Assessing crop coefficients of sunflower and canola using two-source energy balance and thermal radiometry", *Agricultural Water Management* , 137, 23–29, 2014.

Smagorinsky J., "General circulation experiments with the primitive equations. Part I, The basic experiment", *Monthly Weather Review*, 91 (3), 99-164, 1963.

Stengel, M., Kniffka, A., Meirink, J.F., Lockhoff, M., Tan, J. & Hollmann, R. "CLAAS: the CM SAF cloud property dataset using SEVIRI". *Atmospheric Chemistry and Physics*. 14, 4297–4311 , 2014.

Szuromi P., Jasny B., Clery D., Austin J., Hanson B., "Energy for the long haul", *Science*, 315 (5813):781, 2007.

Wilks, D. S., 2006. Statistical Methods in the Atmospheric Sciences, Academic Press, 627 pp.

Wittmann, M., Breitkreuz, H., Schroedter-Homscheidt, M., Eck, M., "Case-Studies on the Use of Solar Irradiance Forecast for Optimized Operation Strategies of Solar Thermal Power Plants". IEEE J. Selected Topics Appl. Earth Observations Remote Sens. 1 (1), 18– 27, 2008.

Zahumensky, I., 2004: World Guidelines on Quality Control Procedures for Data from Automatic Weather Stations. World Meteorological Organization.

Atmos. Meas. Tech. Discuss., doi:10.5194/amt-2017-9, 2017
Manuscript under review for journal Atmos. Meas. Tech.
Discussion started: 23 February 2017

Atmospheric Measurement Techniques Discussions
Open Access

Tables and Figures

Table 1: RAMS grid-setting for the first and second grids. NNXP, NNYP and NNZP are the number of grid points in the west-east, north-south, and vertical directions. Lx(km), Ly(km), Lz(m) are the domain extension in the west-east, north-south, and vertical directions. DX(km) and DY(km) are the horizontal grid resolutions in the west-east and north-south directions. CENTLON and CENTLAT are the geographical coordinates of the grid centers.

	First grid	Second grid
NNXP	231	401
NNYP	231	401
NNZP	36	36
Lx	2772 km	1600 km
Ly	2772 km	1600 km
Lz	≈22 km	≈22 km
DX	12 km	4 km
DY	12 km	4 km
CENTLAT (°)	42.0	42.0
CENTLON (°)	12.5	12.5

Atmos. Meas. Tech. Discuss., doi:10.5194/amt-2017-9, 2017
Manuscript under review for journal Atmos. Meas. Tech.
Discussion started: 23 February 2017

Table 2: Station names, abbreviations, coordinates, height above the sea level (meters, forth column), instrument type and managing institution for the twelve sites.

Station name	Abbreviation	Coordinates (lon;lat)	Height (m) a.s.l	Pyranometer type	Institution
Trapani	tra	12.5; 37.9	9	CM11 Kipp&Zonen	Aeronautica Militare
Cozzo Spadaro	csp	15.1; 36.7	51	CM11 Kipp&Zonen	Aeronautica Militare
Santa Maria di Leuca	sml	18.3; 39.8	112	CM11 Kipp&Zonen	Aeronautica Militare
Capo Palinuro	pal	15.3; 40.0	185	CM11 Kipp&Zonen	Aeronautica Militare
Pratica di Mare	pdm	12.5; 41.7	32	CM11 Kipp&Zonen	Aeronautica Militare
Vigna di Valle	vdv	12.2; 42.1	266	CM11 Kipp&Zonen	Aeronautica Militare
Pisa	pis	10.4; 43.7	6	CM11 Kipp&Zonen	Aeronautica Militare
Cervia	cer	12.3; 44.2	10	CM11 Kipp&Zonen	Aeronautica Militare
Trieste	tri	13.8; 45.7	4	CM11 Kipp&Zonen	Aeronautica Militare
Monte Cimone	cim	10.7; 44.2	2173	CM11 Kipp&Zonen	Aeronautica Militare
Paganella	pag	11.0; 46.2	2129	CM11 Kipp&Zonen	Aeronautica Militare
Aosta	aos	7.4; 45.7	583	CMP21 Kipp&Zonen	Arpa Valle D'Aosta

Table 3: Percentage of data in clear, contaminated and overcast conditions for all stations and seasons, as well as for the whole year, estimated by CPP (Section 2.1).

Station	Winter [%]	Spring [%]	Summer [%]	Fall [%]	Year [%]
tra	48;23;29	/	82;15;03	38;39;23	60;24;16
csp	13;34;53	46;19;35	69;22;09	34;31;35	44;26;30
sml	33;31;36	37;40;23	62;31;07	41;37;22	44;34;20
pal	03;28;69	13;30;57	49;37;14	23;34;43	25;33;42
pdm	36;27;37	37;44;19	79;14;07	51;27;22	54;27;19
vdv	37;25;38	27;45;28	73;20;07	48;29;23	51;28;21
pis	34;22;45	38;33;29	77;16;07	44;29;27	52;24;24
cer	33;20;47	41;27;32	74;16;10	39;25;36	49;22;29
tri	20;21;59	31;29;40	64;24;12	34;23;43	42;24;34
cim	05;50;45	09;46;45	34;49;17	21;36;43	20;45;35
pag	23;22;55	39;27;34	45;38;17	27;31;42	35;31;34
aos	12;39;49	25;35;40	32;38;30	25;38;37	23;37;40

Table 4: rRMSE [%] for the MSG-GHI estimate computed for hourly and daily integrated GHI for different seasons and stations.The first number in each cell is the rRMSE computed using hourly data, the second number is the rRMSE computed for daily integrated GHI, the third number is the rRMSE computed after the MOS correction to the model output for daily integrated GHI (see text for details).

Station	Winter [%]	Spring [%]	Summer [%]	Fall [%]	Year [%]
tra	30; 3; 3	/	11; 4; 4	27; 5; 6	18; 6; 7
csp	20; 5; 3	14; 4; 4	9; 4; 3	19; 3; 6	14; 6; 6
sml	27; 4; 4	21; 6; 6	14; 5; 4	23; 6; 7	19; 8; 8
pal	25; 4; 3	20; 5; 5	11; 4; 4	39; 4; 5	23; 7; 7
pdm	28; 3: 3	17; 5; 5	12; 4; 4	19; 6; 7	17; 7; 7
vdv	27; 3; 3	24; 5; 5	18; 6; 6	24; 4; 6	21; 8; 8
pis	26; 4; 3	22; 6; 5	16; 6; 5	20; 4; 5	19; 7; 7
cer	27; 4; 4	21; 6; 5	15; 6; 5	23; 3; 6	20; 8; 8
tri	34; 3; 3	28; 6; 6	22; 9; 8	25; 5; 7	26; 10; 10
cim	92; 18; 19	60; 24; 27	43; 23; 21	47; 13; 17	53; 27; 28
pag	57; 12; 10	35; 17; 16	38; 17; 17	43; 12; 11	40; 21; 20
aos	89; 7; 10	43; 12; 9	44; 12; 17	53; 6; 9	51; 15; 17

Atmos. Meas. Tech. Discuss., doi:10.5194/amt-2017-9, 2017
Manuscript under review for journal Atmos. Meas. Tech.
Discussion started: 23 February 2017

Atmospheric Measurement Techniques Discussions

Table 5: rRMSE [%] for the RAMS-GHI one-day forecast computed for hourly and daily integrated GHI for different seasons and stations. The first number in each cell is the rRMSE computed using hourly data, the second number is the rRMSE computed for daily integrated GHI, the third number is the rRMSE computed after the MOS correction to the model output for daily integrated GHI (see text for details).

Station	Winter [%]	Spring [%]	Summer [%]	Fall [%]	Year [%]
tra	58; 12; 8	/	20; 12; 10	49; 17; 17	33; 21; 19
csp	43; 12; 9	38; 23; 19	19; 11; 10	42; 15; 16	31; 22; 19
sml	57; 14; 11	47; 25; 19	26; 16; 12	42; 15; 13	38; 27; 21
pal	58; 16; 9	54; 25; 20	27; 18; 16	47; 16; 16	41; 28; 25
pdm	60; 14; 11	48; 28; 21	25; 15; 14	40; 12; 13	37; 27; 22
vdv	66; 14; 10	57; 28; 19	32; 19; 16	49; 14; 14	42; 29; 23
pis	68; 15; 10	56; 28; 21	32; 22; 18	51; 17; 17	45; 30; 25
cer	68; 13; 10	52; 26; 19	34; 20; 16	53; 14; 13	44; 29; 23
tri	97; 16; 11	63; 26; 19	44; 26; 20	58; 16; 15	53; 35; 27
cim	117; 22; 22	96; 44; 44	60; 39; 30	74; 24; 24	75; 48; 44
pag	86; 15; 10	77; 50; 28	66; 44; 26	79; 30; 30	72; 56; 36
aos	113;17; 17	78; 49; 25	71; 48; 43	84; 23; 23	81; 60; 42

Table 6: RMSE [W/m^2] for the RAMS-GHI one-day forecast (first number in each cell), one-day persistence forecast (second number in each cell) and RAMS-GHI one-day forecast after the MOS application computed on a hourly basis for different seasons and stations (third number in each cell, see text for details). Bold style shows the cases when the RAMS-GHI one-day forecast has a worse performance compared to the 1D persistence forecast.

Station	Winter [W/m^2]	Spring [W/m^2]	Summer [W/m^2]	Fall [W/m^2]	Year [W/m^2]
tra	**149**; 120; 130	/	111; 136; 104	**177**; 162; 163	152; 190; 139
csp	137; 169; 126	199; 218; 184	107; 168; 102	168; 191; 157	161; 204; 148
sml	151; 170; 133	218; 275; 200	142; 178; 128	159; 186; 147	178; 236; 160
pal	138; 177; 125	232; 257; 212	145; 181; 141	173; 192; 161	186; 229; 171
pdm	140; 151; 123	226; 231; 206	133; 172; 132	144; 167; 139	176; 209; 161
vdv	138; 161; 115	230; 238; 196	168; 189; 158	158; 170; 140	182; 209; 159
pis	**125**; 119; 104	**227**; 223; 200	165; 180; 153	163; 174; 150	188; 216; 166
cer	**120**; 118; 100	204; 241; 182	170; 206; 158	**149**; 147; 139	178; 220; 157
tri	**131**; 77; 181	**207**; 195; 181	206; 223; 189	**147**; 142; 134	190; 220; 166
cim	**158**; 145; 160	288; 289; 288	253; 274; 220	**199**; 193; 183	253; 293; 238
pag	**148**; 95; 114	**318**; 266; 239	**304**; 291; 255	**224**; 156; 183	**286**; 276; 221
aos	**172**; 99; 148	**341**; 234; 256	326; 347; 281	**200**; 126; 176	287; 294; 229

Atmos. Meas. Tech. Discuss., doi:10.5194/amt-2017-9, 2017
Manuscript under review for journal Atmos. Meas. Tech.
Discussion started: 23 February 2017

Atmospheric Measurement Techniques Discussions
Open Access

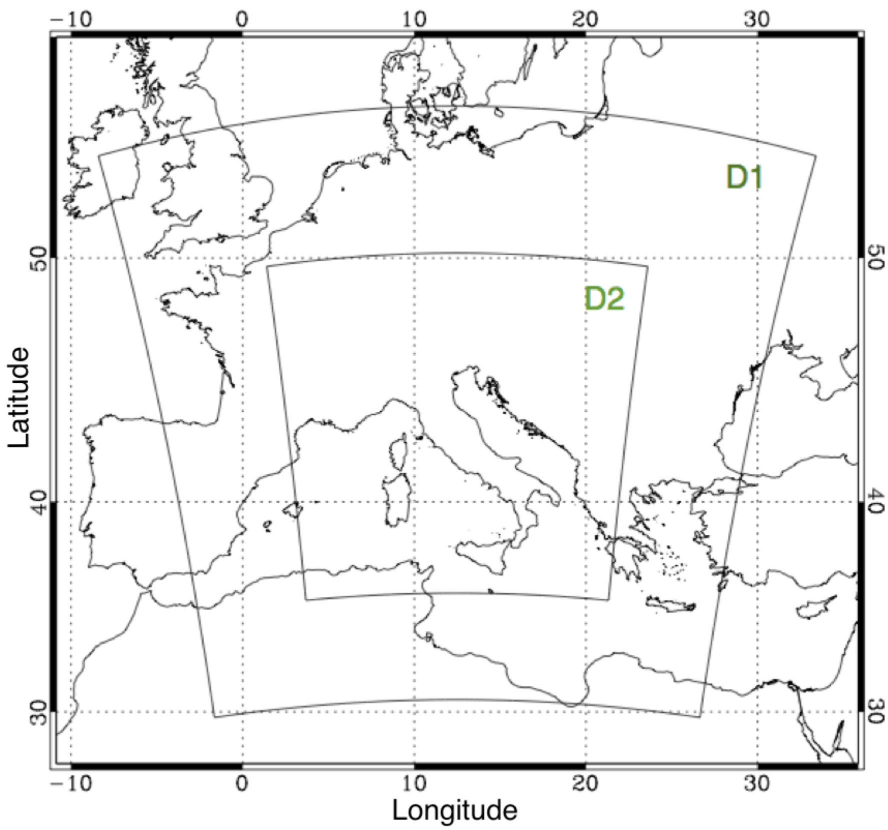

Figure 1: Model domains. The second domain has 4 km horizontal resolution and is nested in the first domain, at 12 km horizontal resolution, using one-way nesting.

Atmos. Meas. Tech. Discuss., doi:10.5194/amt-2017-9, 2017
Manuscript under review for journal Atmos. Meas. Tech.
Discussion started: 23 February 2017

Atmospheric Measurement Techniques
Discussions

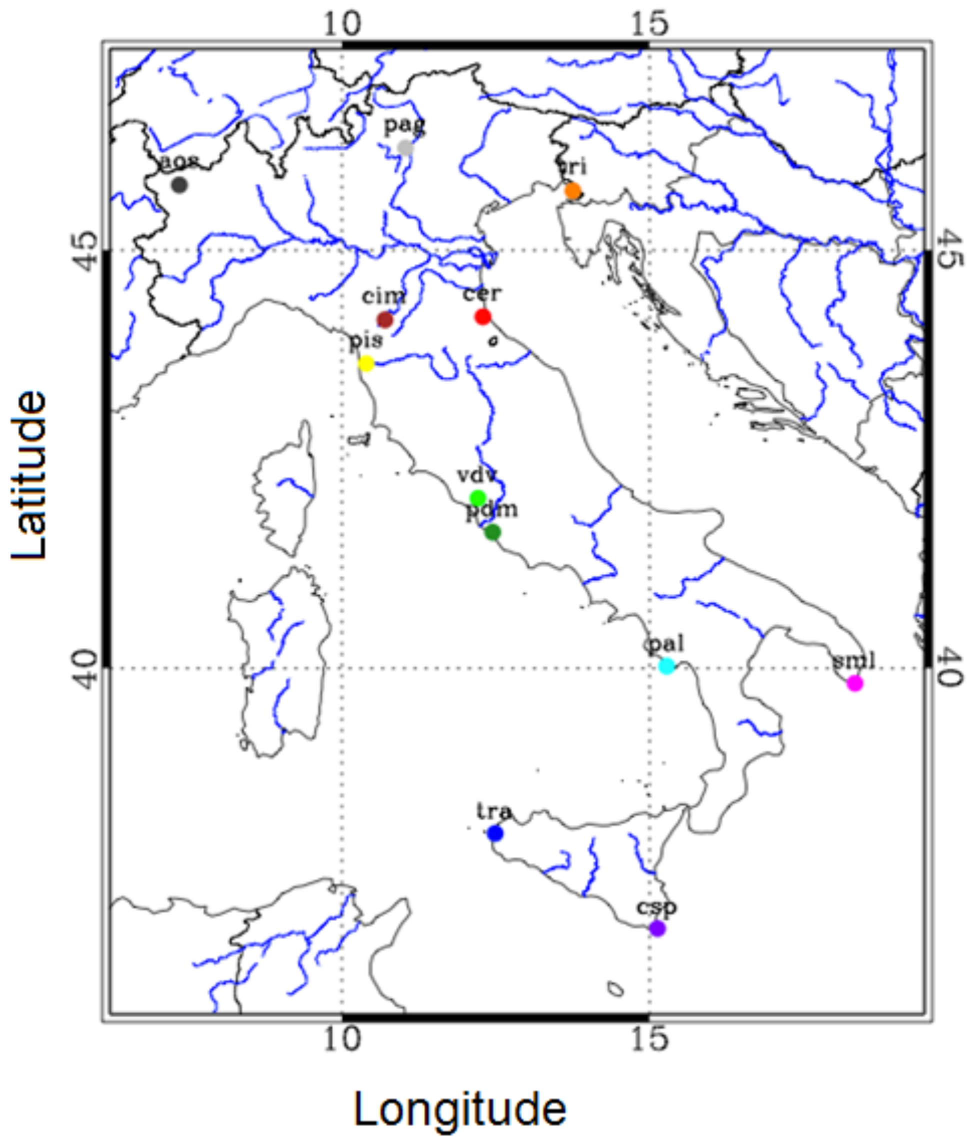

Figure 2: Stations distribution over the Italian territory.

Atmos. Meas. Tech. Discuss., doi:10.5194/amt-2017-9, 2017
Manuscript under review for journal Atmos. Meas. Tech.
Discussion started: 23 February 2017

Atmospheric Measurement Techniques
Open Access
Discussions

a)

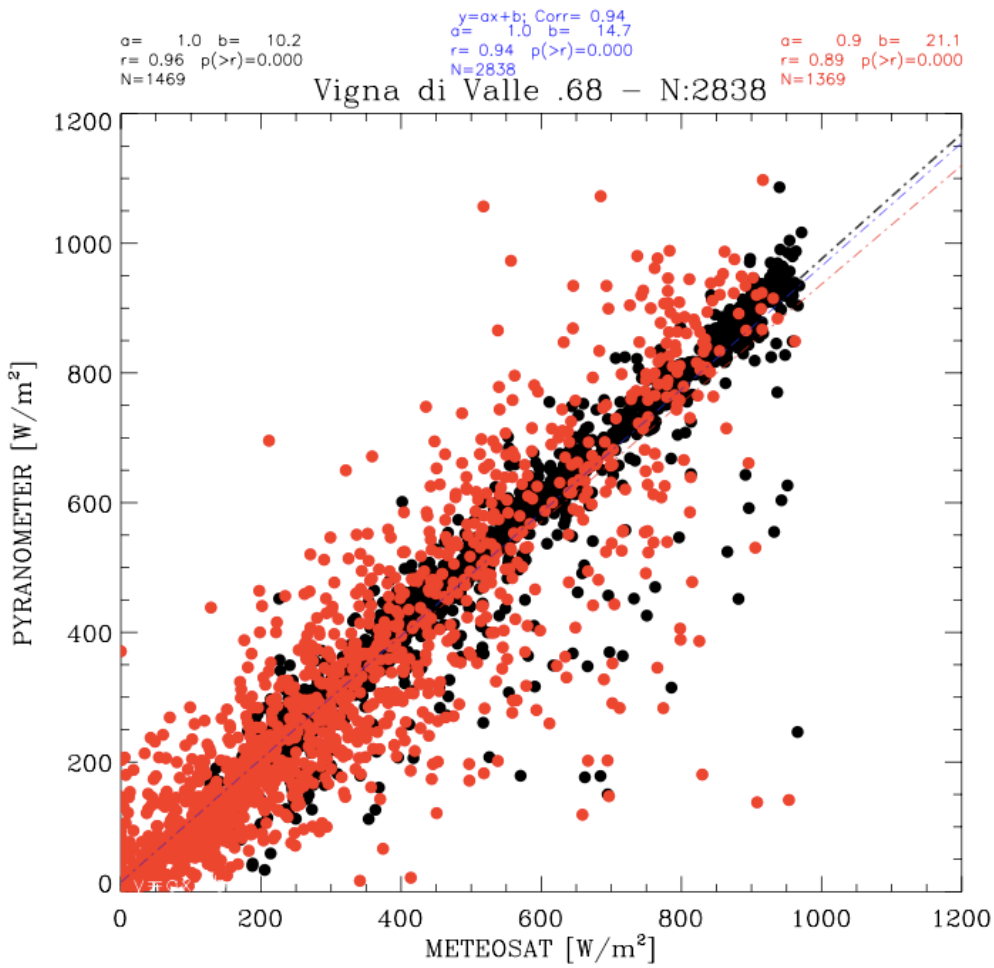

Atmos. Meas. Tech. Discuss., doi:10.5194/amt-2017-9, 2017
Manuscript under review for journal Atmos. Meas. Tech.
Discussion started: 23 February 2017

Atmospheric Measurement Techniques
Open Access
Discussions

b)

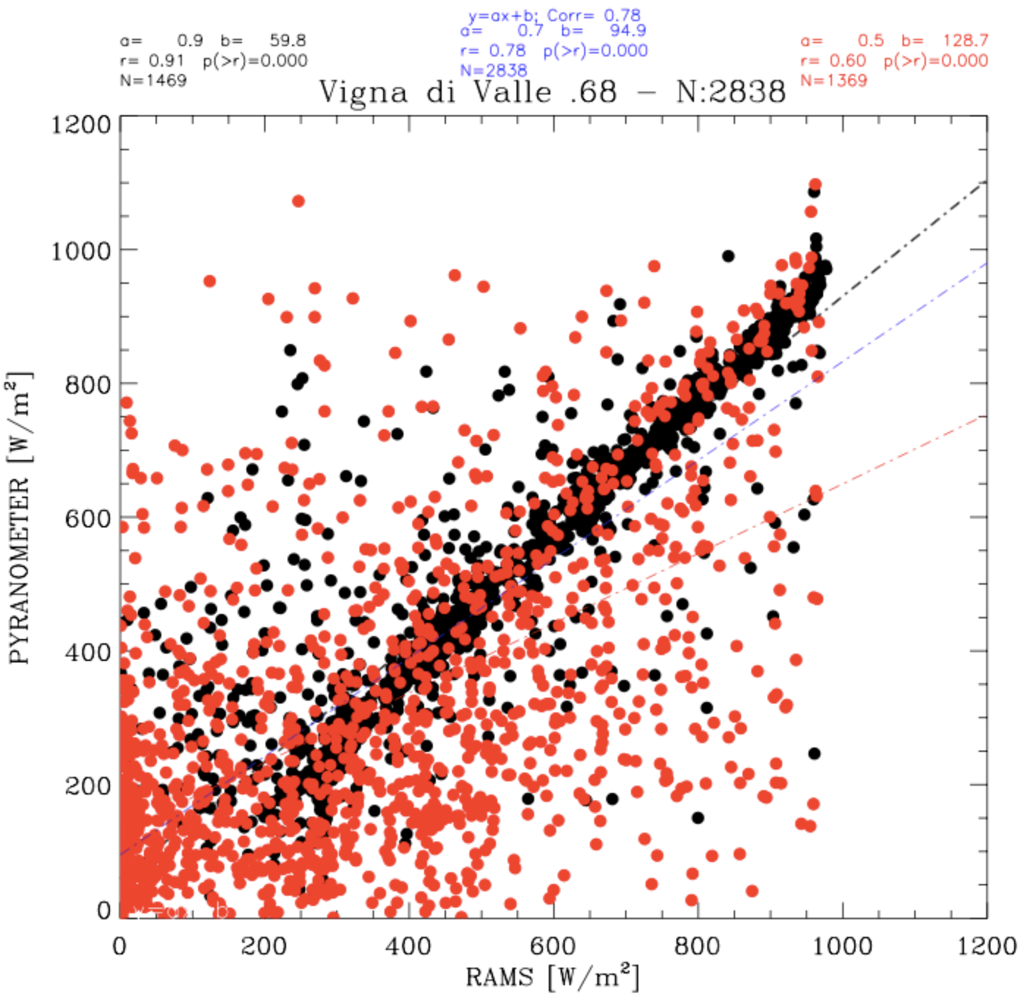

Figure 3: a) scatter plot of the GHI for the MSG (x-axis) and the pyranometer (y-axis). The black dots are for clear sky conditions while the red dots are for both contaminated and overcast skies; b) as in a) for the RAMS one-day forecast.

a)

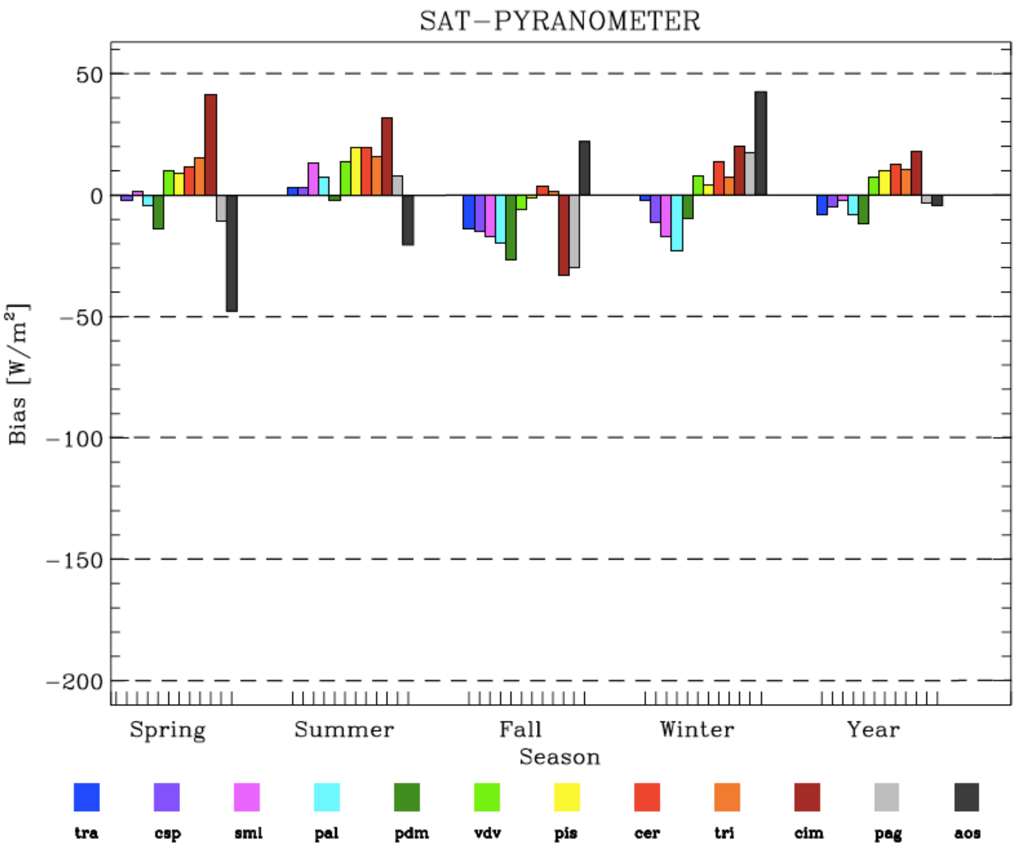
SAT−PYRANOMETER
Bias [W/m²]
50
0
−50
−100
−150
−200
Spring
Summer
Fall
Winter
Year
Season
tra
csp
sml
pal
pdm
vdv
pis
cer
tri
cim
pag
aos

b)

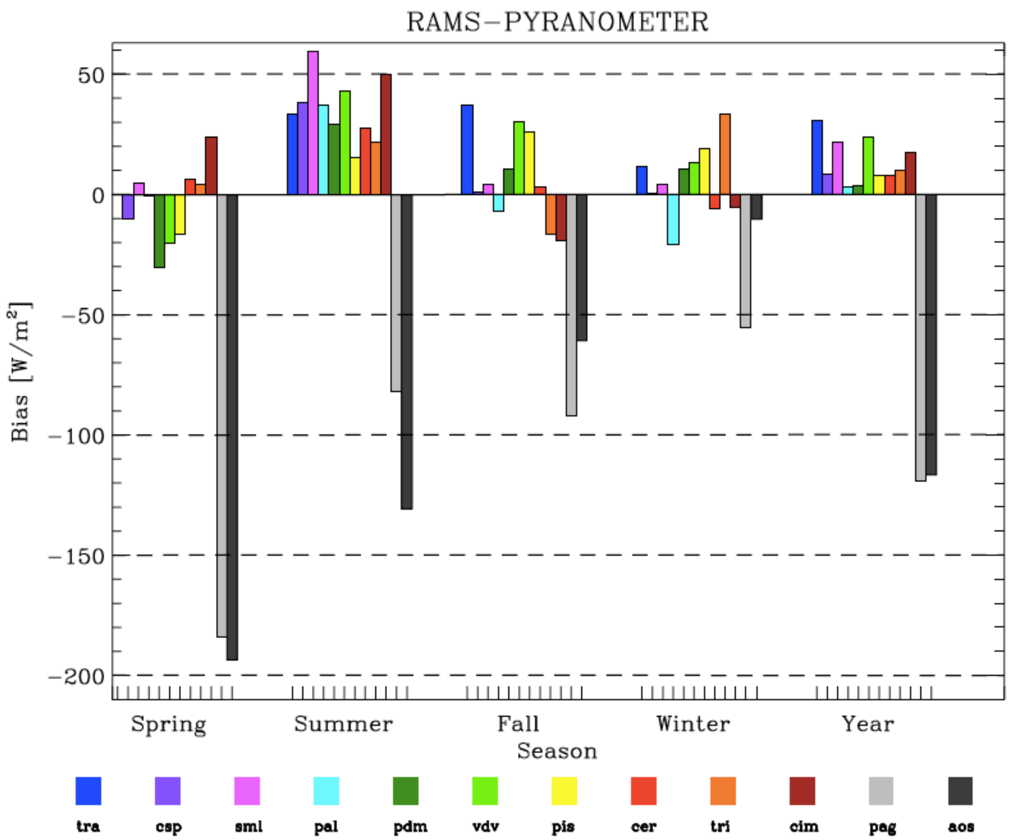

Fig. 4: a) MBE for the MSG-GHI for the different stations and seasons as well as for the whole year. The figure has been derived from the hourly data of pyranometers and MSG-GHI estimate; b) As in Figure 4a for the RAMS forecast.

Atmos. Meas. Tech. Discuss., doi:10.5194/amt-2017-9, 2017
Manuscript under review for journal Atmos. Meas. Tech.
Discussion started: 23 February 2017

Atmospheric Measurement Techniques
Open Access
Discussions

a)

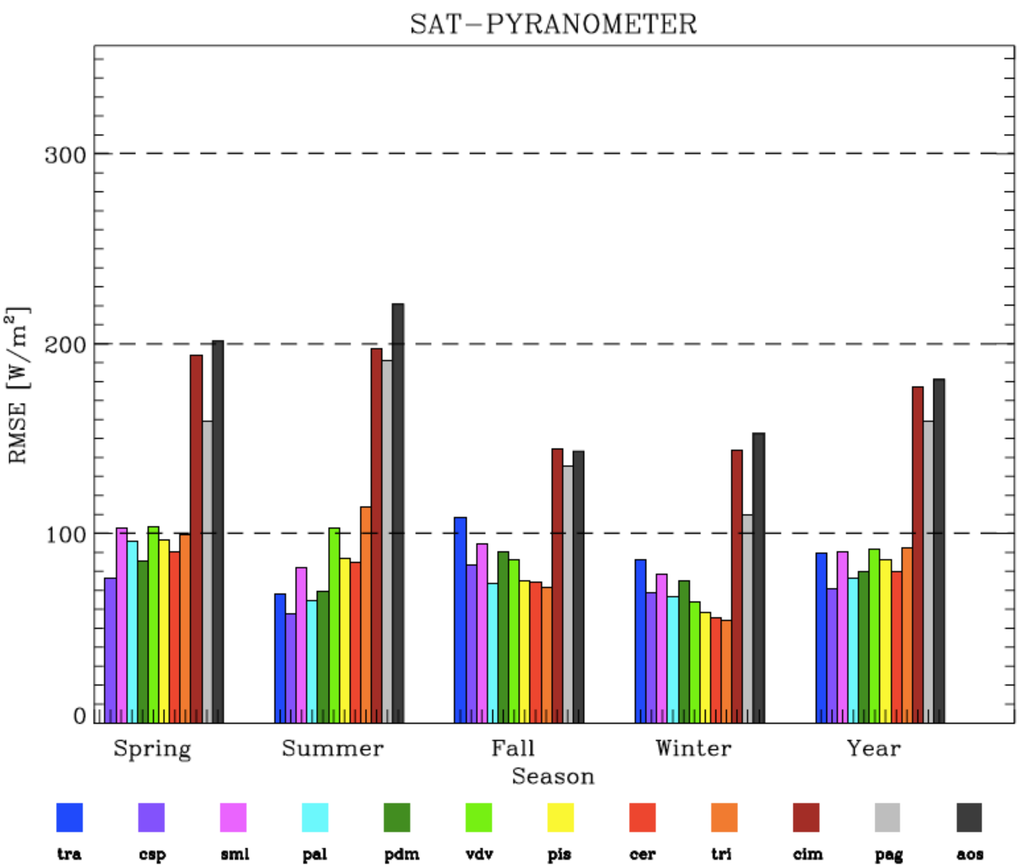

Atmos. Meas. Tech. Discuss., doi:10.5194/amt-2017-9, 2017
Manuscript under review for journal Atmos. Meas. Tech.
Discussion started: 23 February 2017

Atmospheric Measurement Techniques
Open Access
Discussions

b)

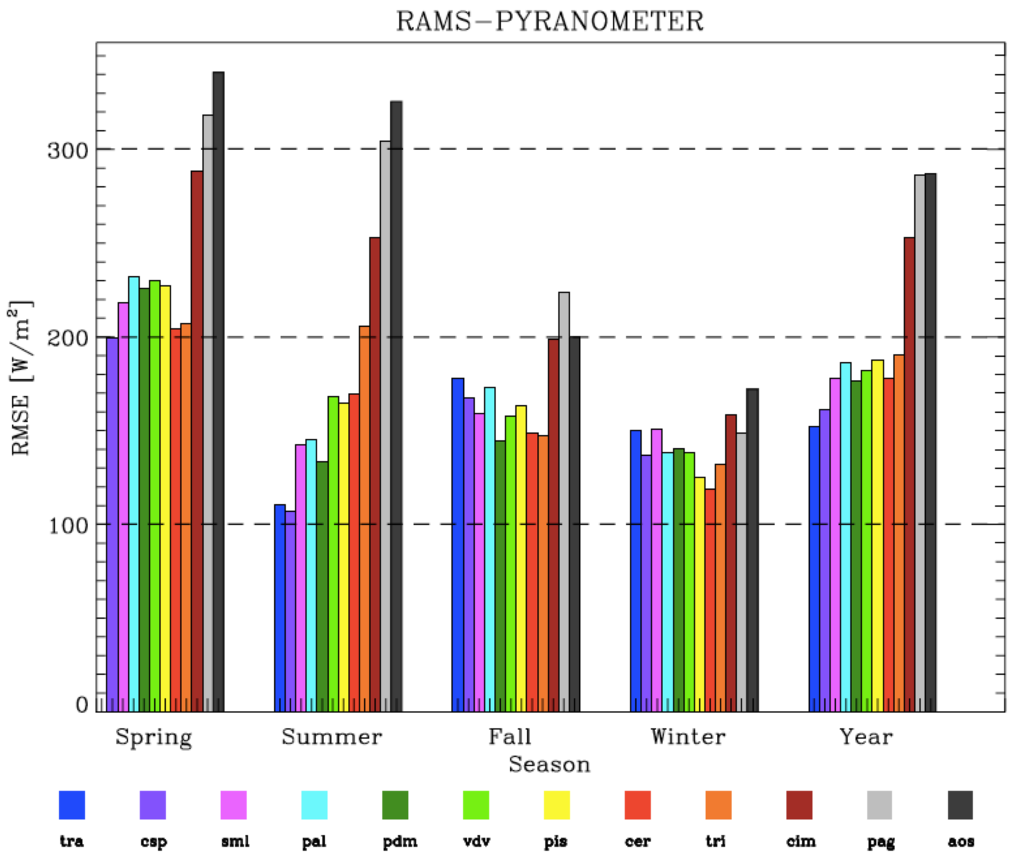

Fig. 5: a) RMSE for the MSG-GHI for the different stations and seasons as well as for the whole year. The figure has been derived from the hourly data of pyranometers and MSG-GHI estimate; b) As in a) for the RAMS forecast.

Atmos. Meas. Tech. Discuss., doi:10.5194/amt-2017-9, 2017
Manuscript under review for journal Atmos. Meas. Tech.
Discussion started: 23 February 2017

Atmospheric Measurement Techniques
Discussions
Open Access

a)

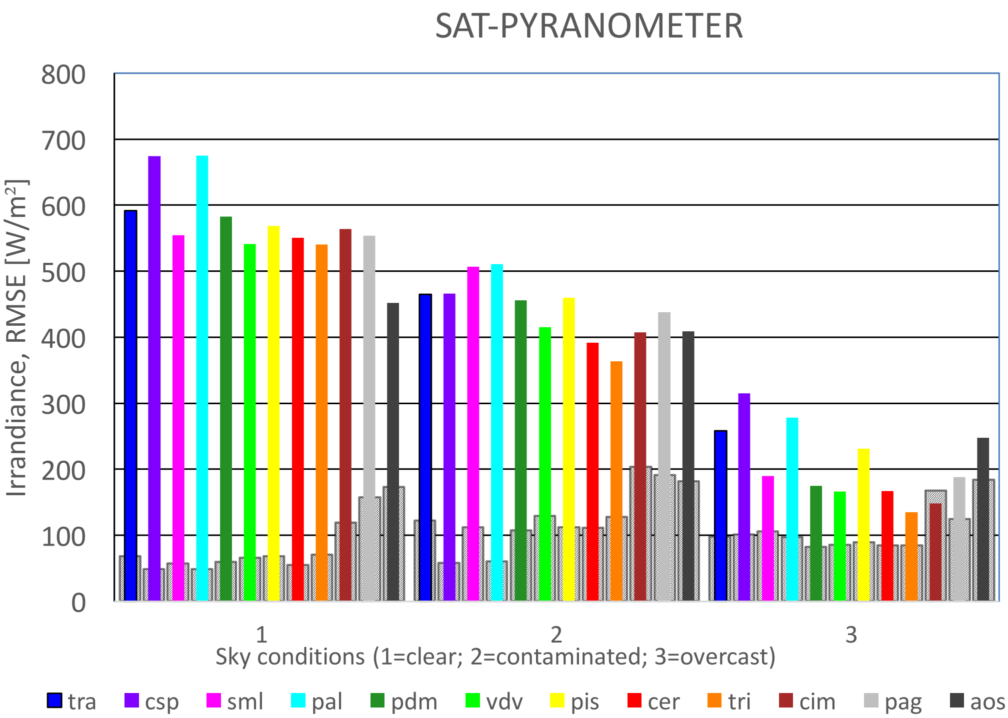

Atmos. Meas. Tech. Discuss., doi:10.5194/amt-2017-9, 2017
Manuscript under review for journal Atmos. Meas. Tech.
Discussion started: 23 February 2017

b)

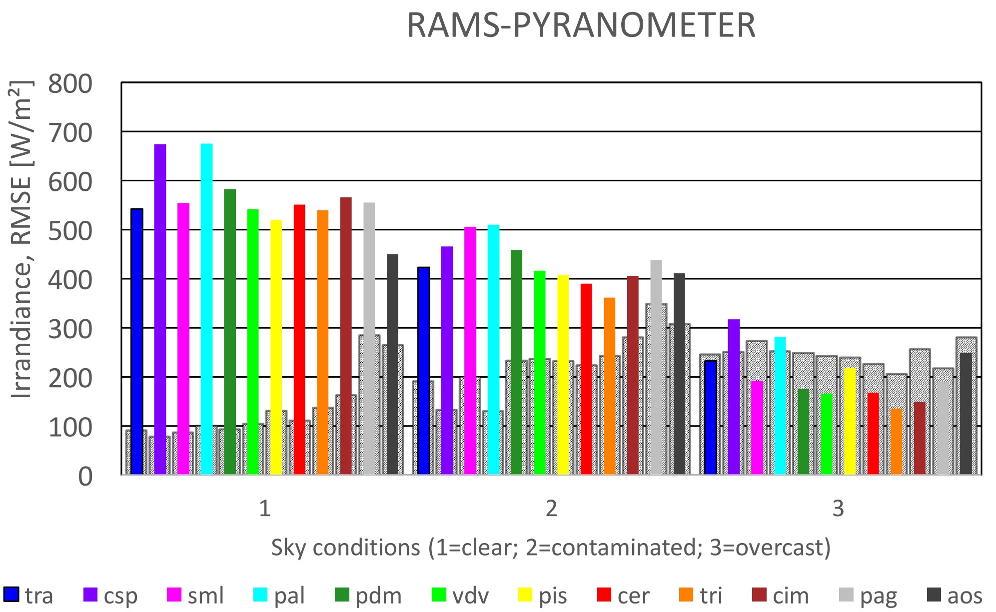

Figure 6: a) Mean irradiance (coloured bars) and RMSE for different sky conditions: clear (1), contaminated (2) and overcast (3) for the MSG-GHI estimate. The figure has been derived from the hourly data of pyranometers and MSG-GHI estimate. The RMSE is shown by the gray bars in the background with the same scale as the mean irradiance; b) As in a) for the RAMS-GHI one-day forecast.

a)

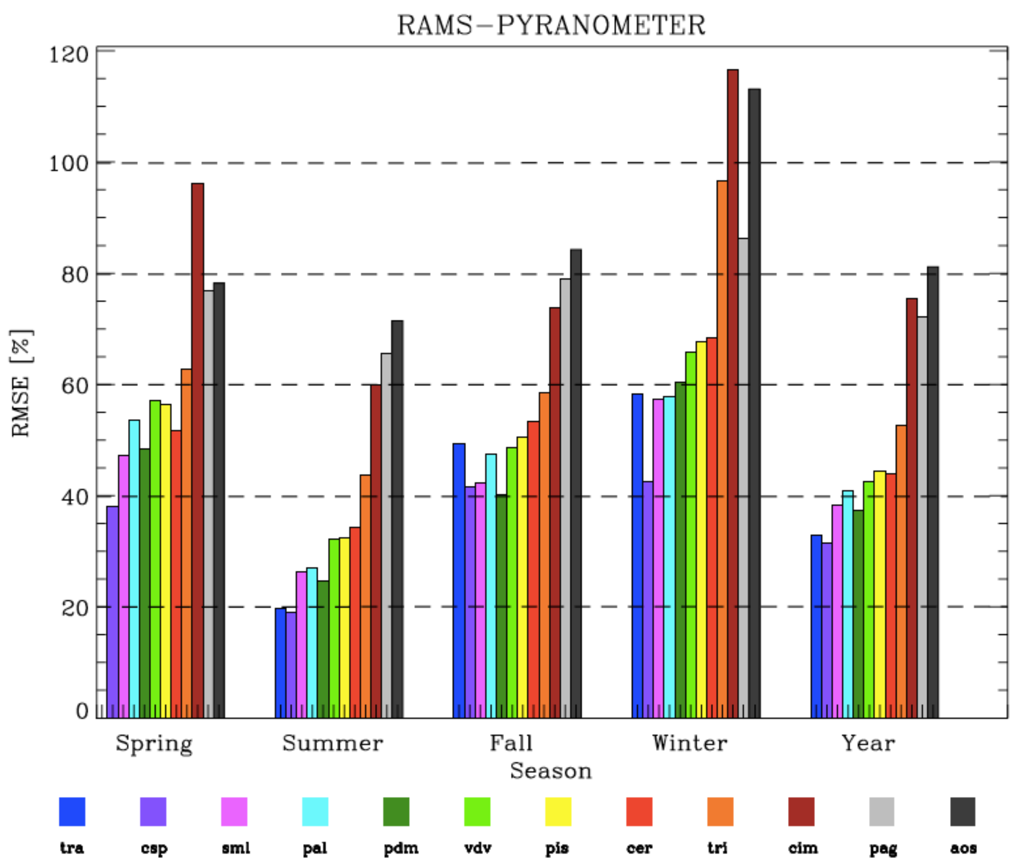
RAMS–PYRANOMETER
RMSE [%]
0
20
40
60
80
100
120
Spring
Summer
Fall
Winter
Year
Season
tra
csp
smi
pal
pdm
vdv
pis
cer
tri
cim
pag
aos

Atmos. Meas. Tech. Discuss., doi:10.5194/amt-2017-9, 2017
Manuscript under review for journal Atmos. Meas. Tech.
Discussion started: 23 February 2017

765 b)

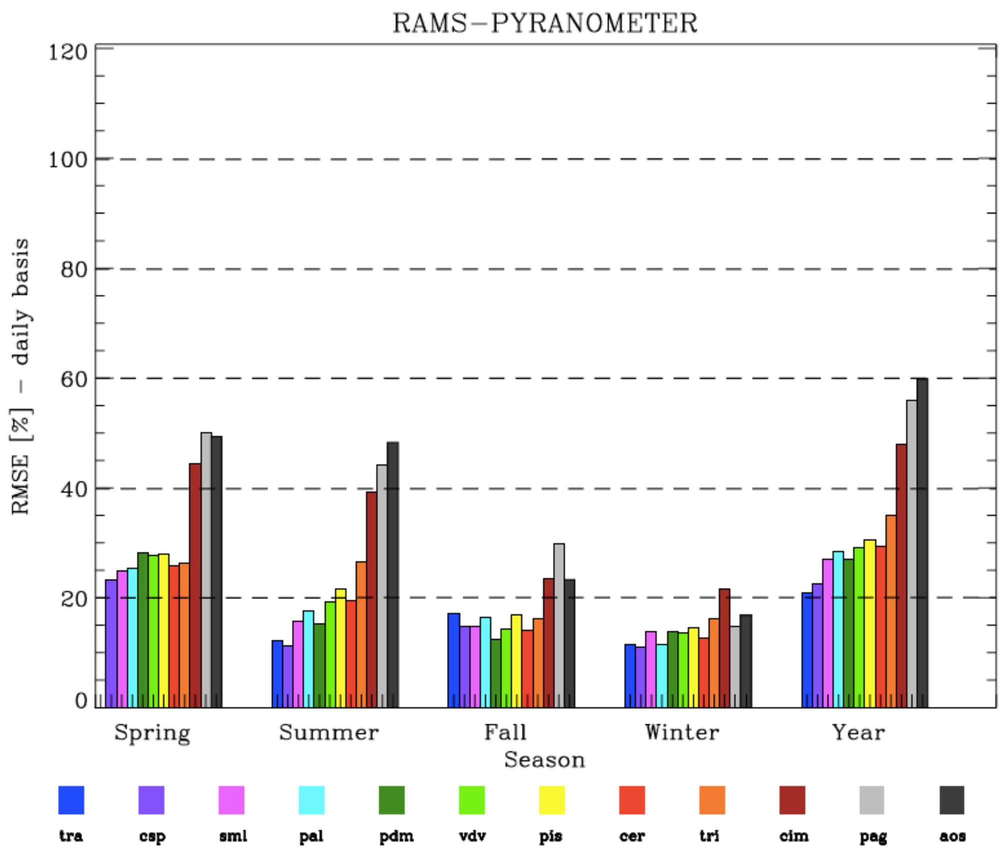

766

Atmos. Meas. Tech. Discuss., doi:10.5194/amt-2017-9, 2017
Manuscript under review for journal Atmos. Meas. Tech.
Discussion started: 23 February 2017

Atmospheric Measurement Techniques Discussions
Open Access

767 **c)**

768 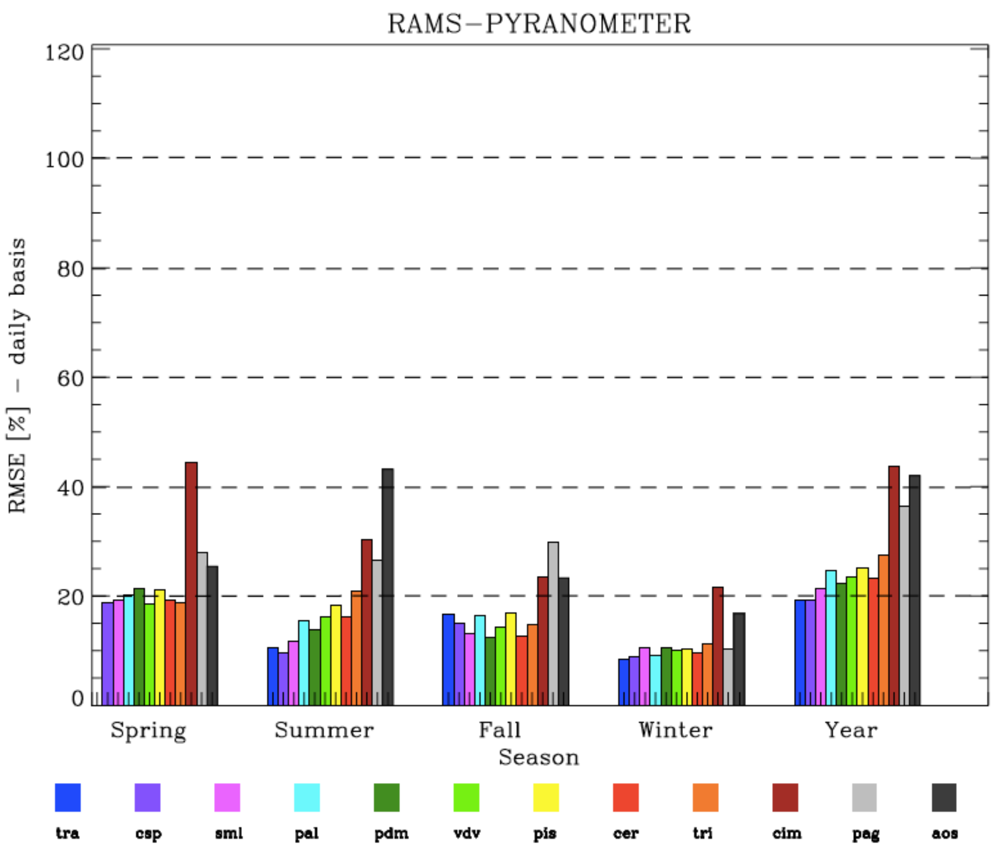

769

770 Figure 7: a) rRMSE computed for different seasons and stations, as well as for the whole year, for
771 the RAMS-GHI one-day forecast starting from hourly data; b) as in a) for daily integrated GHI; c)
772 as in b) after the MOS correction to the model output for daily integrated GHI.

773